Fracture process analyses of small-scaled concrete columns in controlled blasting utilizing simplified charge holder and steel plate ring

Hakman Kim[*], Sangho Cho[**†], Daisuke Fukuda[***], Sewook Oh[**],
Gyeongjo Min[**], Hoon Park[**], and Katsuhiko Kaneko[****]

[*]Geotechnical Engineering Research Institute, Korea Institute of Civil Engineering and Building Technology,
Daehwa-Dong, Ilsanseo-Gu, Goyang-Si, Gyeonggi-Do, 10223, SOUTH KOREA

[**]Department of Mineral Resources & Energy Engineering, Chonbuk National University, Deokjin-Dong, Jeonju-City,
Jeollabuk-Do, 561−756, SOUTH KOREA
Phone: +82−63−270−4636
[†]Corresponding author: chosh@jbnu.ac.kr

[***]Faculty of Engineering, Hokkaido University, Kita 13 Nishi 8, Kita-ku, Sapporo-shi, Hokkaido, 060−8628 JAPAN

[****]Horonobe Research Institute for the Subsurface Environment, 5−3 Sakae, Horonobe, Teshio-gun, Hokkaido,
098−3221 JAPAN

Abstract

A dynamic breakage system for the removal of a cylindrical concrete pile head by means of controlled blasting method using diamond shaped charge holder the hollow steel plate is experimentally and numerically examined to prove the effectiveness of hollow steel plate as a crack arrester for the purpose of minimization of the damages in the remaining part of concrete pile. In order to prove the effectiveness of hollow steel plate as a crack arrester for the purpose of minimization of the damages in the remaining part of concrete pile, blast experiments and numerical analyses were conducted by DFPA-A code. The experimental and numerical results clearly showed that the case with the steel plate resulted in better fracture pattern in which the damage in the remaining concrete pile below the steel was reduced, while the case without the steel plate resulted in significant fracturing toward remaining part of concrete pile. In order to investigate the influence of both the loading rate characterized by rise time of the applied pressure and spacing between steel plate and charge hole on the resultant fracture pattern, the laboratory-scale experiment of concrete pile head by blasting a cylindrical charge with a hollow steel plate was conducted.

1. Introduction

Deep foundations generally include piles, drilled shafts, caissons and piers. In many countries, drilled shafts have been utilized as a foundation of ground structures such as apartments, skyscrapers and bridges[1] because these can resist both axial and lateral loads and minimize the settlement of the foundation. However, in the case of cast-in-place concrete piles, the top part of the concrete pile, i.e.

concrete pile head, should be adjusted to the bottom level of main foundation. In addition, the strength decreasing of the pile head occurs because of laitance. Thus, the breakage of concrete pile head is required. However, the breakage of concrete pile head by the conventional mechanical methods involves with various risks with respect to safety not only for site workers but also for general public living in the vicinity, mainly due to noise
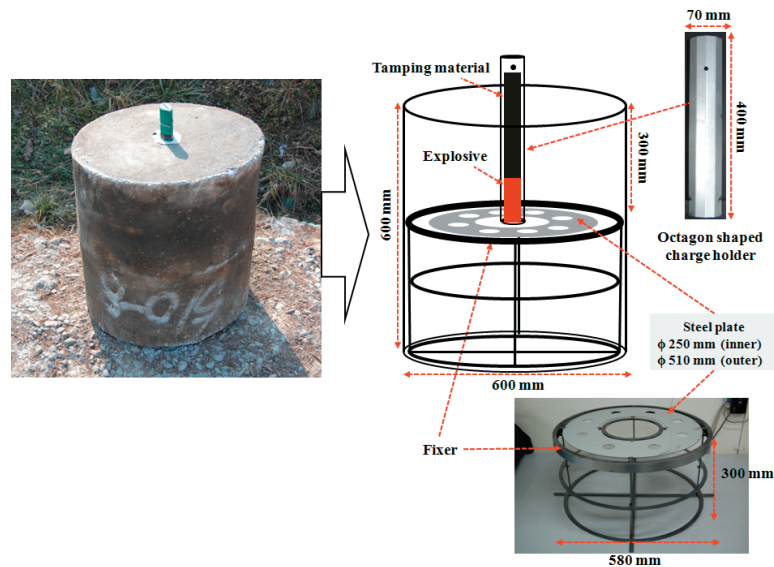
Figure 1   Description of the specimen used in the blasting experiments.

hazard. Therefore, alternative methods to solve the problem have been required[2]. Many researchers proposed a new alternative method[3)–6)], i.e. a dynamic breakage system for concrete pile head utilizing a charge holder and steel plate for controlling crack propagation to prevent the damage occurring at remaining part of concrete pile by blasting.

In the remaining part of concrete pile, conical cracks from bottom of charge hole, i.e. damages on a lower part of concrete pile, occurred in laboratory-scale experiment. The effectiveness of the dynamic breakage system was proved in both laboratory-scale and field-scale blast experiments. Although these experimental results were successful, it was difficult to understand the detailed mechanism of crack growth occurring inside the concrete pile and to find the optimum designs such as the best shape of the charge holder and the best installation location of crack arrester. For this purpose, the Dynamic Fracture Process Analysis (DFPA) for 2 dimensional (2-D) problem has been proposed and applied to the simulation of blasting. However, to understand fracture pattern and detailed knowledge of 3 dimensional (3-D) fracture process for each technique is required.

However, cylindrical charge is frequently applied[7] and corresponding geometrical representation of the problem in case of utilizing detonation or deflagration of explosive for fragmentation of rock-like materials can be considered as axisymetry. As pointed out through the verification of Dynamic fracture process analysis for axisymmetric problem (DFPA-A) proposed by Kim et al.[8], the 3-D propagation of conical cracks from the bottom corner of the charge hole can occur and investigation of control of this crack is of significant importance in terms of the prevention of the damage in the remaining concrete pile after the removal of the pile head. However, conventional DFPA for 2-D problem[9–16)] cannot analyze this problem and thus DFPA-A[8] proposed and developed can be applicable for the investigation of the effectiveness of crack arrester in the dynamic breakage system for

removing the top of the cylindrical concrete pile.

In this study, the dynamic breakage system for the removal of a cylindrical concrete pile head by blasting with the hollow steel plate is experimentally and numerically investigated to prove the effectiveness of hollow steel plate as a crack arrester for the purpose of minimization of the damages in the remaining part of concrete pile. Then, assuming the laboratory-scale experiment of concrete pile head removal by blasting a cylindrical charge with a hollow steel plate, DFPA-A is conducted to investigate the influence of both the loading rate and spacing between steel plate and charge hole on the resultant fracture pattern, and the obtained fracture patterns are compared.

2. Fracture controlled blast experiments of small scaled concrete columns
2.1 Preparation of concrete column specimens and blast experiments

In order to understand the applicability of the hollow steel plate in the dynamic breakage system for the removal of a cylindrical concrete pile head by blasting proposed by Nakamura et al.[3], a laboratory-scale experiment is conducted. Figure 1 shows the information of the specimen used in the experiment. A cylindrical concrete pile with both the diameter and height of 600 mm is prepared in which both the octagon shaped charge holder and hollow plate made of galvanized steel are installed. The inner and outer diameters of the hollow steel plate are 250 mm and 510 mm, respectively, and its thickness is 1.5 mm. The fixer made of steel is also used for the purpose of the reduction of shock wave generated from charge holder. For charge conditions, the seismic electronic detonator (No.8) and an explosive called "New Fineker" made by Hanwha cooperation, South Korea are used. Then, the space above the New Fineker in the charge holder was filled by the tamping material, i.e. rapidly curing cement. The volumes of the charge holder except tamping material (V_c) and explosive (V_e) are 198.17

(a) Without the hollow steel plate   (b) With the hollow steel plate

Figure 2   Resultant fracture patterns of blasting experiments.
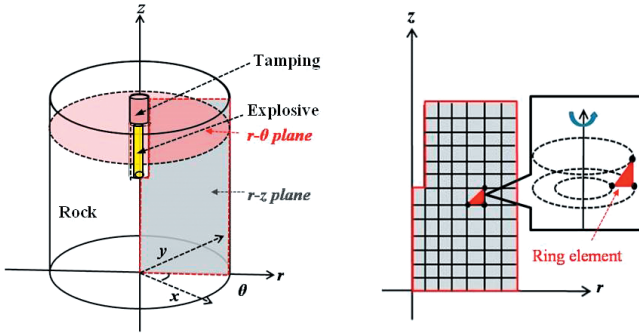
(a) 3-D cylindrical charge model.   (b) Axisymmetric FEM model

Figure 3   Axisymmetric representation of 3-D problem.

cm^3 and 96.21 cm^3, respectively. Therefore, the volumetric decoupling ratio defined by V_c / V_e is 2.06, resulting in relatively slower rise time of the generated pressure. The uniaxial compressive strength of concrete is 41 MPa. Then, the resultant fracturing pattern is observed. For the comparison, the fracturing pattern in the concrete specimen without the application of the hollow steel plate is also conducted.

2.2 Experiment results

The fracture patterns obtained from the experiments for the cases with/without the application of the steel plate is shown in Figure 2. As is evident, the case without the steel plate results in the crack propagation to the bottom part of concrete, i.e. the damage in the remaining part of concrete pile. On the other hand, the case with the steel plate results in well-controlled crack pattern, i.e. no crack toward the bottom part of concrete pile. In addition, the upper part of the specimen in both cases, i.e. concrete pile head, is split into two pieces because the charge holder has the two slits at the opposite sides where the large stress concentration due to the application of detonation pressure occurs. From these results, the effectiveness of steel plate on controlling fractures and minimizing the damages of remaining part of the concrete pile is indicated. However, with only these experiments, the identification of ideal type of explosive, i.e. characteristics of applied pressure wave form, and installation location of the steel plate to minimize the damage to the remaining concrete pile is difficult to investigate.

3. Axisymetric fracture process analyses of small scaled blast experiments
3.1 Description of dynamic fracture simulation method for axisymmetric problem

In the DFPA-A, a 3-D cylindrical charge model shown in

Figure 3(a) is analyzed. The figure is shown by cylindrical coordinate (r, θ, z) where z coincides with the axial direction of the charge hole, and r and θ are polar coordinates at the cross section perpendicular to the z axis. Because the geometrical representation of the model is axisymmetric with respect to z axis, u_θ in the displacement components (u_r, u_θ, u_z) becomes zero. Thus, only u_r and u_z need to be considered, resulting in the configuration of FEM mesh shown in Figure 3(b) with the domain discretization by triangular ring elements[17]. For this model, the following equation of motion for axisymmetric problem is solved :

$$\frac{\partial \sigma_{rr}}{\partial r} + \frac{\sigma_{rr} - \sigma_{\theta\theta}}{r} + \frac{\partial \sigma_{zr}}{\partial z} = \rho \frac{\partial^2 u_r}{\partial t^2}$$
$$\frac{\partial \sigma_{rz}}{\partial r} + \frac{\sigma_{rz}}{r} + \frac{\partial \sigma_{zz}}{\partial z} = \rho \frac{\partial^2 u_z}{\partial t^2} \quad (1)$$

where $\{\sigma_k\} = \{\sigma_{rr}, \sigma_{zz}, \sigma_{\theta\theta}, \sigma_{rz}\} (k = 1, 2, 3, 4)$ are Cauchy stress components and ρ, the density. As a constitutive equation, the visco-elastic behavior is modeled as :

$$\{\sigma_k\} = D_{kl} \left\{ \varepsilon_l + \eta \frac{\partial \varepsilon_l}{\partial t} \right\} (k, l = 1, 2, 3, 4) \quad (2)$$

where $\{\varepsilon_k\} = \{\varepsilon_r, \ \varepsilon_z, \ \varepsilon_\theta, \ 2\varepsilon_{rz}\} (k = 1, 2, 3, 4)$ are infinitesimal strain components, D_{kl}, the elastic coefficients for isotropic materials determined from Young's modulus and Poisson's ratio, and η, the damping constant. In addition, the strain-displacement relation is given as :

$$\{\varepsilon_k\} = \sum_{I=1}^{3} \sum_{j=1}^{2} (B_I)_{kj} \cdot u_{jI} (k, l = 1, 2, 3, 4) \quad (3)$$

where I is local node number in each ring element, $(B_I)_{kj}$, coefficients determined from mesh geometry, and u_{jI} the nodal displacements where $j = 1$ and 2 indicate r and z directions, respectively[17]. From Equations (1)–(3), the resulting finite element equation was solved with the help of new-mark β method[18] for time discretization. The nodal acceleration, velocity and displacement as well as stresses and strains were dynamically updated to express a large deformation due to crack opening.

As is evident from Equation (2), there are 3 principal stress components, i.e. two components are in a plane spanned by r- and z-axes and the other component in θ direction. Thus, fracturing process must be 3-dimentionally considered. The tensile fracturing occurring within the plane spanned by r- and z-axes (hereafter, r-z tensile fracture) and toward r-θ direction (hereafter, r-θ tensile fracture) was modeled. In addition, the compressive fracturing was newly modeled in the following manner.

For the r-z tensile fracture, the inter element cracking method shown in Figure 3(a) was used where the crack initiation, propagation and coalescence were expressed by element separations when the induced stress normally acting on element-boundary exceeded the given tensile strength. This approach was shown to be quite useful and realistic for complex fracturing simulation[19]. After the crack initiation, non-linear crack opening behavior due to the existence of fracture process zone near the crack tip was considered. The bi-linear model of tensile softening

law characterized by the cohesive traction, T, of each crack face and crack opening displacement (COD) as shown in Figure 4(a) was used.

For the r-θ tensile fracture, aforementioned inter element cracking method cannot be applied due to 2-D nature of the axisymmetric formulation. In addition, the COD traction based tensile softening law cannot be used because of the requirement of $u_\theta = 0$ in the axisymmetric problem. Thus, as shown in Figure 4(b), the r-θ tensile fracture was treated in each element and an approach base on stress-strain relation was used to express a decohesion of crack toward θ direction. In this approach, a circumferential stress (σ_θ)−strain (ε_θ) relation was expressed by a linear elastic behavior when the induced stress level was below the given tensile strength, T_t. Then, after the induced stress level exceeded T_t, as shown in Figure 5(a), the stress-strain relation corresponding to the decohesion process characterized by bi-linear model of strain softening law was used instead of COD traction relation. For the evaluation of strains ε_1 and ε_2 in Figure 5
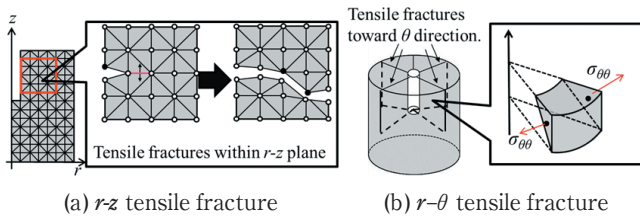
(b), the method proposed by Kim et al.[8] was used which utilized the number of virtual radial predominant cracks from a cylindrical charge hole, N, with recourse to the fracturing pattern analyzed from the 2-D dynamic fracture process analysis[8] under a plane-strain condition. Thus, for example, the value of N is 4 in Figure 5(b) because there are four predominant θ-tensile fractures. In the following analysis, $N = 5$ was assumed.

The compressive fracturing was modeled in each element as elastic-perfectly plastic behavior. Mohr−Coulomb yield function and Drucker-Prager plastic potential were used for the judgment of compressive fracture initiation and expression of post-fracture behavior, respectively. Because rocks are heterogeneous material, this research modeled the rock heterogeneity by a microscopic tensile strength distribution following Weibull's distribution characterized by coefficient of uniformity[20]. Here, although the concept of heterogeneity in the axisymmetric problem showed a contradiction in that the axisymmetry with respect to z axis required the strength distribution to be axisymmetric in the plane spanned by r- and z-axes for each θ. However, according to Kim et al.[8], the influence of heterogeneity in this regard has a minor role on the resulting fracture pattern and was neglected.

3.2 Model description and analysis conditions

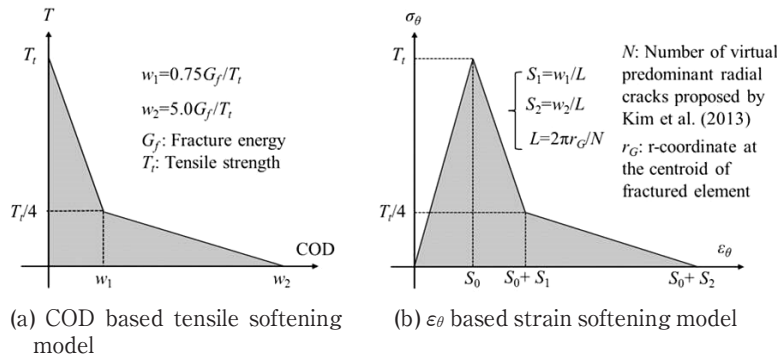To simulate the dynamic fracturing process in cylindrical concrete pile, the DFPA-A assuming the same

(a) *r-z* tensile fracture   (b) *r-θ* tensile fracture

Figure 4   Axisymmetric FEM model.

(a) COD based tensile softening model

(b) ε_θ based strain softening model

Figure 5   Model for non-linear crack opening behavior.
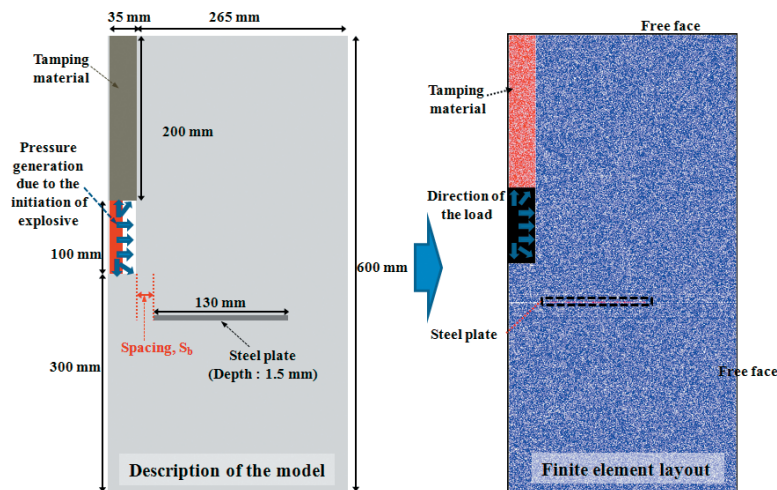
Figure 6   Description of the finite element mesh having a hollow steel plate.

Materials	Parameters	Value
Concrete	Density, ρ [kg m^{-3}]	2170
	Elastic modulus, E [GPa]	36.17
	Poisson's ratio, ν	0.25
	Mean tensile strength, S_t [MPa]	4
	P wave velocity, V_p [m s]	4500
	S wave velocity, V_s [m s]	2601
	Coefficient of uniformity, m	5
Steel plate	Density, ρ [kg m^{-3}]	7900
	Elastic modulus, E [GPa]	207
	Poisson's ratio, ν	0.33
	Mean tensile strength, S_t [MPa]	290
	P wave velocity, V_p [m s]	6100
	S wave velocity, V_s [m s]	3500

Table 2 Condition of the analysis models.

Case	Maximum pressure, P_0 [MPa]	Rise time, t_0 [μs]	Spacing between steel plate and harge hole, S_b [mm]
1	100	10	90
2	100	50	90
3	100	100	90
4	100	50	5
5	100	50	15
6	100	50	35
7	100	50	65
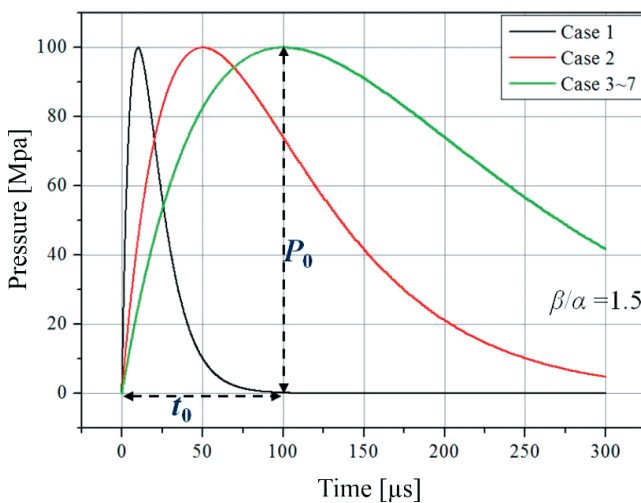
Figure 7 Pressure-time curve for applied pressure waveform for Table 2.

experimental configuration as in Figure 2 is conducted and the fracture mechanism is numerically investigated in detail. In Figure 6, a model of cylindrical concrete pile with a cylindrical charge hole and hollow steel plate is shown with the size information and corresponding FEM mesh. In the mesh generation, the size of each 3-node triangular ring element is set to be small enough to avoid the mesh dependency of crack path. The analysis model has three free faces on the upper, lateral and bottom part of model.

The total number of elements and initial nodes are 79247 and 40000, respectively. The physical properties of the concrete and steel plate which are experimentally determined are listed in Table 1. As is evident from the table, it is assumed that the no fracturing occur in the steel plate which is justified from the experimental result in Figures 2(a) and 2(b). In addition, the physical properties of tamping material are assumed to be same as steel plate and its strength is set large enough not to allow the crack propagation into the tamping material. In the following, the DFPA-As with/without the application of the steel plate are conducted. Then, the influence of both t_0 and the distance between charge hole and steel plate, S_b, on the resultant fracture pattern, and the obtained fracture patterns are compared for each case in Table 2. Figure 7 shows the pressure-time curve for applied pressure waveforms in each case in Table 2. The strength on the boundary between the steel plate and concrete is expressed by that of concrete. For the applied pressure $P(t)$ at time t, the following equation is used to investigate the influence of both maximum pressure and rise time on the fracture pattern[21] :

$$P(t) = P_0\xi\{\exp(-\alpha t)-\exp(-\beta t)\} \quad (4)$$

$$\xi = 1/\{\exp(-\alpha t_0)-\exp(-\beta t_0)\} \quad (5)$$

where α and β are constants, ξ, normalization constant, P_0, maximum pressure and t_0, rise time of the pressure. $P_0 = 100$ MPa is used for all analyses in this chapter. The t_0 is given in the following form :

$$t_0 = \{1/(\beta-\alpha)\}\log(\beta/\alpha) \quad (6)$$

where $\beta/\alpha = 1.5$ is used for all analyses.

3.3 Fracture process and fracture pattern

In Figure 8, the result of DFPA-A, i.e. the progress of tensile fracturing without/with the steel plate, is shown from $t = 0$ to 150 μs. The result corresponding to Case 3 is chosen considering the volumetric decoupling ratio and S_b used in the experiment. In the figure, the tensile fracturing occurring in both *r-z* and *r-θ* planes (hereafter, *r-z* and *r-θ* tensile fractures, respectively) introduced in Chapter 3 are expressed in solid black lines and red regions, respectively. The *r-z* and *r-θ* tensile fractures include the fracture process zone and opened fracture. In Figure 8(a), around 15 μs, it is observed that both the *r-z* and *r-θ* tensile fractures are initiated from the side wall of the charge hole. Then, at $t = 45$ μs, the predominant *r-z* tensile fractures extending obliquely upward and downward from the top and bottom corners of the charge hole, respectively, are found. The mechanism of the occurrence of these predominant fractures, i.e. conical cracks, was already discussed in Chapter 3. Then, between $t = 45$ to 105 μs, these conical cracks continued extending. In addition, *r-θ* tensile fractures mainly occur in the way that the conical cracks surround the *r-θ* tensile fractures for these time intervals. It is also noted that, after around $t = 105$ μs, both the initiation and downward propagation of the conical cracks and *r-θ* fractures are also found from

(a) Without the hollow steel plate   (b) Installation of the hollow steel plate
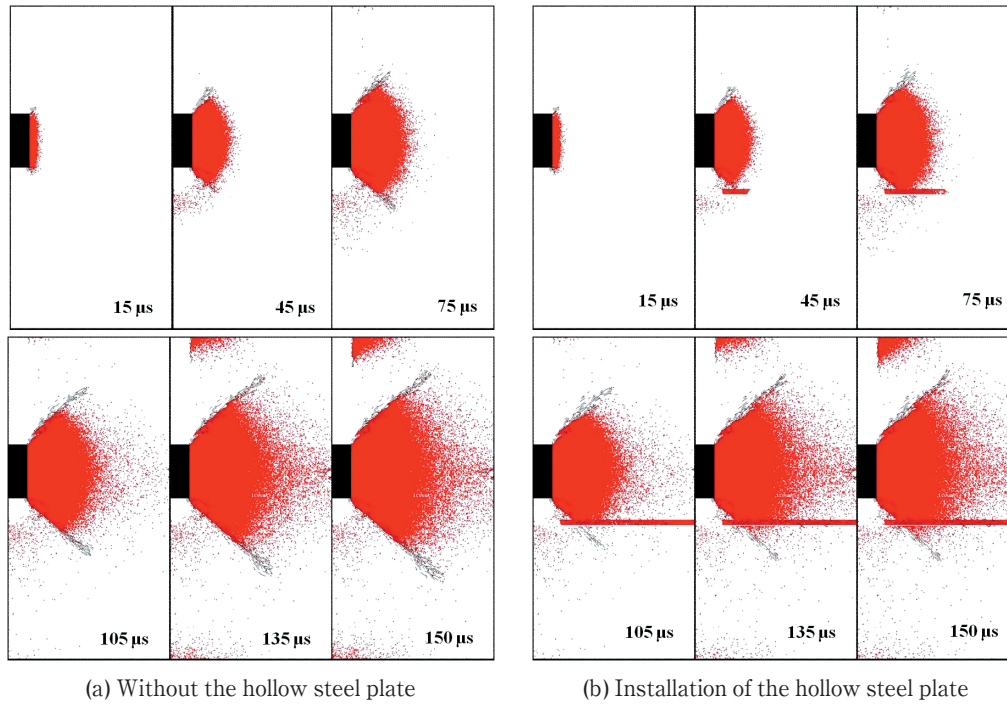
Figure 8   Result of fracture process in with/without the hollow steel plate.

top outer boundary of concrete pile. At around $t = 150$ μs, the r-θ tensile fractures almost reach at the lateral outer free face of the model, resulting in splitting the specimen by r-θ tensile fracture as well as the occurrence of two predominant conical cracks form the top and bottom corners of charge hole.

On the other hand, Figure 8(b) shows the result of DFPA-A with the steel plate from $t = 0$ to 150 μs. Similar to the case without the steel plate, at around $t = 15$ μs, the predominant conical cracks from the bottom and top corners of the charge hole are found. The conical crack extending upward shows the similar propagation manner because no crack arrester is used in this direction. However, the conical crack extending downward starts interacting with the steel plate at around $t = 45$ μs. Then, although the minor extension of the conical crack below the steel plate is still observed, the resultant length of this conical crack is clearly reduced by the existence of the steel plate. In addition, comparing the r-θ tensile fracturing in the cases with/without the steel plate, the r-θ tensile fractures with the steel plate clearly results in the less fracturing below the steel plate and the effectiveness of steel plate to reduce the damage in the remaining part of concrete pile is now justified.

4. Discussion
4.1 Influence of applied pressure on fracture pattern

To examine the influence of loading rate on the resultant of fracture pattern, the results of DFPA-A for Cases 1, 2 and 3 in Table 2 are compared, in which all the cases use the same values of P_0 and S_b but different t_0. Figure 9 shows comparison of the resultant fracture patterns for Cases 1, 2 and 3 at $t = 150$ μs. All of these results show that the predominant r-θ tensile fractures occur from the lateral wall of charge hole which are bounded by predominant r-z tensile fractures, i.e. conical
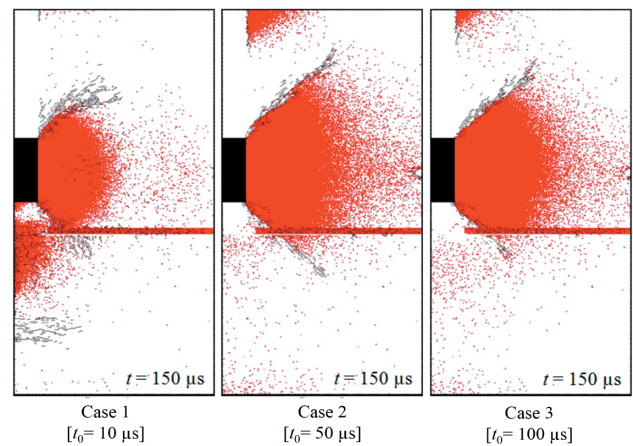
Figure 9   Influence of rise time, t_0, on the resultant fracture pattern [$P_0 = 100$ MPa, $S_b = 90$ mm].

cracks initiated from the bottom and top corners of charge hole. The fracturing occurring above the steel plate is more or less similar to each other with minor differences around the top free face. By comparing these three cases in terms of the degree of damage in the remaining part of concrete pile below the steel plate, Case 1 with the shortest rise time results in the worst fracture pattern in which the intense r-θ and r-z tensile fractures occur just below the bottom of charge hole although the r-θ tensile fractures and conical crack from the bottom corner of charge hole is not significant below the steel plate. On the other hand, Case 3 with the longest rise time results in the shortest conical crack and least r-θ tensile fractures occurring below the steel plate. Case 2 also shows the similar result to that of Case 3 with slightly longer conical crack and slightly more intense r-θ tensile fractures below the steel plate. Therefore, in case that the t_0 is considered as variable, blasting conditions with the larger t_0 than 50 μs is more effective for arresting the conical crack

Case 4
[s_b = 5 mm]

Case 5
[s_b = 15 mm]

Case 6
[s_b = 35 mm]

Case 7
[s_b = 65 mm]
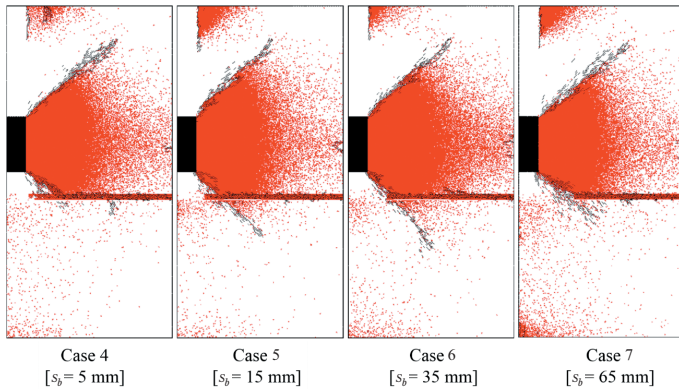
Figure 10 Influence of spacing between steel plate and charge hole, S_b, on fracture pattern [P_0 = 100 MPa, t_0 = 50 μs].

propagation and to preventing the damages in the remaining part of concrete pile below the steel plate. In addition, it is also indicated that larger t_0 can results in less r-θ tensile fractures below the steel plate.

4.2 Influence of spacing between steel plate and charge hole on fracture pattern

To examine the influence of S_b on the resultant fracture pattern, the DFPA-A for Cases 4, 5, 6 and 7 in Table 2 are compared, in which all the cases use the same values of P_0 and t_0 but different S_b. Figure 10 shows the comparison of the resultant fracture patterns for Cases 4, 5, 6 and 7 at t = 150 μs. All of these results show that the predominant r-θ occur from the lateral wall of charge hole which are bounded by predominant r-z tensile fractures, i.e. conical cracks initiated from the bottom and top corners of charge hole. The fracturing occurring above the steel plate is quite similar to each other with minor differences around the top free face. By comparing the four cases in terms of the degree of damage in the remaining part of concrete pile below the steel plate, Case 4 with the shortest S_b results in the best fracture pattern in which little conical crack and r-θ tensile fractures occur below the steel plate. On the other hand, Cases 5, 6 and 7 with relatively larger S_b result in longer conical crack and more or less r-θ tensile fractures occurring below the steel plate because the interaction of crack propagation from the charge hole with the steel plate is compromised in these cases. Therefore, in case that the S_b is considered as variable, blasting conditions with the installation distance of the hollow steel plate less than 5 mm from charge hole is more effective for arresting the conical crack propagation to the remaining part of concrete pile below the steel plate. In addition, it is also indicated that smaller S_b can also result in less r-θ tensile fractures below the steel plate.

5. Conclusions

A dynamic breakage system by blasting with a hollow steel plate as a crack arrester proposed by Nakamura et al.[3] for the removal of a cylindrical concrete pile head was experimentally and numerically investigated.

First, to prove the effectiveness of hollow steel plate as a crack arrester for the purpose of minimization of the damages in the remaining part of concrete pile, two types of experiments and DFPA-As with/without the application of the steel plate were conducted. The experimental and numerical results clearly showed that the case with the steel plate resulted in better fracture pattern in which the damage in the remaining concrete pile below the steel was reduced, while the case without the steel plate resulted in significant fracturing toward remaining part of concrete pile.

Then, to investigate the influence of both the loading rate characterized by rise time t_0 of the applied pressure and spacing between steel plate and charge hole, S_b, on the resultant fracture pattern, various DFPA-As assuming the laboratory-scale experiment of concrete pile head by blasting a cylindrical charge with a hollow steel plate was conducted and the obtained fracture patterns were compared

In case that the t_0 is considered as variable, blasting conditions with the larger t_0 than 50 μs was found to be more effective for arresting the conical crack propagation and prevention of the damages in the remaining part of concrete pile below the steel plate. In addition, it was indicated that the larger t_0 could result in less r-θ tensile fractures below the steel plate. On the other hand, in case that the S_b was considered as variable, blasting conditions with the installation distance of the hollow steel plate less than 5 mm from charge hole was found to be more effective for arresting the conical crack propagation to the remaining part of concrete pile below the steel plate. Therefore, considering all the DFPA-A results, the application of loading condition which realizes the relatively slower loading rate, i.e. $t_0 > 50$ μs, and $S_b < 5$ mm should be used to obtain the optimized fracture pattern.

References
1) Y. Won, J. Lee, Y. Kim, and S. Park, Architectural Institute of Korea, 18, 181−190 (2002).
2) I. Takatoshi, M. Masanori, and S. Mitsuru, The World Tunnel Congress and 32nd ITA Aseembly, 22−27 (2006).
3) M. Kato, Y. Nakamura, Y. Ogata, M. Yamamoto, and T. Matsuzawa, Kayaku to hoen, 39, 26−31 (in Japanese).
4) Y. Nakamura, M. Kato, Y. Ogata, I. Yamaura, S. Nakamura, and S. Cho, 2010, "10th Conference on Japan Society of Civil Engineers", 117−120. (in Japanese).
5) M. Kato, Y. Nakamura, Y. Ogata, S. Kubota, T. Matsuzawa, S. Nakamura, T. Adachi, I. Yamaura, and M. Yamamoto, Sci. Tech. Energetic Materials, 70, 108−111 (2009).
6) S. Nakamura, H. Takeuchi, Y. Nakamura, and T. Higuchi, The 7th International Conference on Explosives and Blasting, 197−208, (2013).
7) K. Sassa and I. Ito, Journal of the Society of Materials Science, 21, 123−129 (1972). (in Japanese).
8) H. Kim, D. Fukuda, J. Ikezawa, K. Moriya, S. Cho, and K. Kaneko, Sci. Tech. Energetic Materials, 74, 74−81 (2013).
9) K. Kaneko, Y. Matsunaga, and M. Yamamoto, Kayaku Gakkaishi (Sci. Tech. Energetic Materials), 56, 207−215 (1995). (in Japanese).
10) M. Yamamoto, T. Ichijo, T. Inaba, K. Morooka, and K. Kaneko, Int. J. Rock Fragmentation by Blasting, 3, 3−24 (1999).

11) S. Cho, Y. Ogata, and K. Kaneko, Int. J. Rock. Mech. Min. Sci., 40, 763−777 (2003).

12) S. Cho, M. Nishi, M. Yamamoto, and K. Kaneko, Mater. Trans, 44, 951−956 (2003).

13) S. Cho and K. Kaneko, Int. J. Rock Mech.Min. Sci., 41, 771−784 (2004).

14) S. Cho, B. Mohanty, M. Ito, Y. Nakamiya, S. Owada, S. Kubota, Y. Ogata, A. Tsubayama, M. Yokota, and K. Kaneko, Int. Proc. 41st US Symposium on Rock Mechanics, Inc., 06−11 Curran Associates (2006).

15) S. Cho, Y. Nakamura, B. Mohanty, H. Yang, and K. Kaneko, Engineering Fracture Mechanics, 75, 3966−3984 (2008).

16) D. Fukuda, K. Moriya, K. Kaneko, K. Sasaki, R. Sakamoto, and K. Hidani, Int. J. Fracture, 180, 163−175 (2012).

17) T. Belytschko, W. Liu, and B. Moran, "Nonlinear Finite Elements for Continua and Structures", 622−623 John Wiley & Sons (2000).

18) N. Newmark, Proc. ASME, 67−94 (1959).

19) J. Song, H. Wang, and T. Belytschko, Comput. Mech. 42, 239−250 (2008).

20) W. Weibull, J. Appl. Mech., 18, 293−297 (1951).

21) W. Duvall, Geophysics, 18, 310−323 (1953).

22) I. Ito and K. Sassa, J. Mining and Metallurgical Institute of Japan, 84, 1059−1065 (1968). (in Japanese).